JOURNAL OF VIROLOGY, Jan. 1997, p. 325–330 Vol. 71, No. 1
0022-538X/97/$04.00+0
Copyright © 1997, American Society for Microbiology

# Three-Dimensional Structure of Infectious Bursal Disease Virus Determined by Electron Cryomicroscopy

B. BÖTTCHER,[1] N. A. KISELEV,[2] V. Y. STEL'MASHCHUK,[2] N. A. PEREVOZCHIKOVA,[3] A. V. BORISOV,[3] AND R. A. CROWTHER[1]*

*Medical Research Council Laboratory of Molecular Biology, Cambridge CB2 2QH, United Kingdom,[1] and Institute of Crystallography, Russian Academy of Sciences, Moscow 117333,[2] and Institute for Animal Health, 600900 Vladimir,[3] Russia*

Received 27 June 1996/Accepted 10 September 1996

**Infectious bursal disease virus (IBDV), a member of the *Birnaviridae* group, is a commercially important pathogen of chickens. From electron micrographs of frozen, hydrated, unstained specimens, we have computed a three-dimensional map of IBDV at about 2 nm resolution. The map shows that the structure of the virus is based on a T=13 lattice and that the subunits are predominantly trimer clustered. The subunits close to the fivefold symmetry axes are at a larger radius than those close to the two- or threefold axes, giving the capsid a markedly nonspherical shape. The trimer units on the outer surface protrude from a continuous shell of density. On the inner surface, the trimers appear as Y-shaped units, but the set of units surrounding the fivefold axes appears to be missing. It is likely that the outer trimers correspond to the protein VP2, carrying the dominant neutralizing epitope, and the inner trimers correspond to protein VP3, which has a basic carboxy-terminal tail expected to interact with the packaged RNA.**

Infectious bursal disease virus (IBDV) is a member of the *Birnavirus* group, so called because the genomes of these viruses consist of two segments of double-stranded RNA (5, 9). It is a commercially important pathogen of young chickens. After infection, IBDV multiplies rapidly in the B lymphocytes of the bursa of Fabricius, leading to immunosuppression and increased susceptibility to other diseases (for a review, see reference 14). Recent virulent strains have resulted in high rates of mortality (6, 19).

Segment A of the RNA (~3.4 kb) codes for a precursor polyprotein, which is proteolytically cleaved to yield three structural proteins of the mature virion (13). These are termed VP2 (~40 kDa), VP3 (~32 kDa); and VP4 (~28 kDa). VP2 and VP3 are major components of the virus, while VP4 is present in smaller amounts. VP2 carries major neutralizing epitopes (1, 2), suggesting that it is at least partly exposed on the outer surface of the capsid. VP3 contains a very basic carboxy-terminal region, which is likely to interact with the packaged RNA and therefore to be on the inside of the capsid (13). Segment B of the RNA (~2.9 kb) codes for the viral RNA polymerase VP1 (~90 kDa), which is packaged in the virion.

Electron microscopy of negatively stained preparations has shown that the virus is an isometric particle with a diameter of about 60 to 65 nm (16). It is nonenveloped and appears to be single shelled. Detailed analysis of images of negatively stained and of shadowed preparations has suggested that the architecture of the capsid of IBDV is based on the geometry of a skew T=13 icosahedral lattice of the right-handed type (T=13d) (16).

We have used electron microscopy of unstained, frozen, hydrated specimens combined with computer image processing to make a three-dimensional map of IBDV at about 2 nm resolution. The advantage of this approach compared with negative staining is that the specimen is preserved in a near-native environment and that the biological material rather than the stain is imaged, so that internal details of the particle can be visualized. The map shows that the capsid of IBDV is based on the architecture of a T=13 lattice, with trimer clustering of the subunits. The overall thickness of the capsid is about 9 nm. At outer radii between 31 and 33 nm, the relative arrangement of trimers produces a honeycomb pattern on the surface of the virus. At inner radii between 26 and 30 nm, the trimers have triangular or Y-shaped profiles and pack more closely to form a nearly continuous shell. The subunits nearest to the fivefold axes lie at a larger radius from the center of the particle than do those around the three- or twofold axes, giving the capsid a markedly nonspherical shape.

## MATERIALS AND METHODS

**Virus preparation.** IBDV (isolate from Archangel, Russia, 1995) was propagated in Lohmann brown chickens. Freshly dissected bursae were homogenized in 0.02 M Tris-HCl, pH 7.8 (10%, wt/vol), and the virus was precipitated with polyethylene glycol (10%, wt/vol). The pellet was resuspended in 0.02 M Tris-HCl–0.15 M NaCl, pH 7.8, and chloroform was added (30%, vol/vol). After centrifugation at 17,000 × *g* for 20 min in a Beckman J2-21 centrifuge, the aqueous phase was collected. The material was further purified by gradient centrifugation (Sorvall OTD-65, AH-627 rotor, 70,000 × *g*, 6 h, 10°C) on CsCl (mean density, 1.37 g/cm$^3$) overlaid with sucrose (mean density, 1.04 g/cm$^3$). Fractions (0.5 ml) were collected and monitored at 280 nm (LKB Uvicord spectrophotometer). Appropriate fractions were dialyzed overnight against 0.01 M Tris-HCl, pH 7.8. The virus was further purified by centrifugation through CsCl (mean density, 1.27 g/cm$^3$), and the pellet was resuspended in 0.02 M Tris HCl, pH 7.8. The virus concentration was estimated spectrophotometrically, and the quality of the material was checked by electron microscopy of negatively stained preparations.

**Cryomicroscopy.** The virus suspension (2 μl) was frozen at room temperature (4, 11) in a controlled-environment freezing device (3). Micrographs were taken under low-dose conditions at a nominal magnification of ×60,000 on a Philips EM420 operating at 120 kV using a Gatan cold stage with a focus level range of 0.5 to 3.5 μm under focus.

**Image processing.** Micrographs were scanned with a modified Joyce Loebl densitometer. A step size of 30 μm/pixel, corresponding to 0.5 nm on the specimen, was used. The orientation of particles was determined initially by using self-common lines (7) and later by using cross-common lines to projections of calculated three-dimensional maps of IBDV (4, 8). After refining the orientation and origin, the relative magnification of each particle image was also determined by cross-common line fitting to the model by using a variable radial scale factor.

* Corresponding author. Mailing address: Medical Research Council Laboratory of Molecular Biology, Hills Road, Cambridge CB2 2QH, United Kingdom. Phone: 44 1223 248011. Fax: 44 1223 213556.

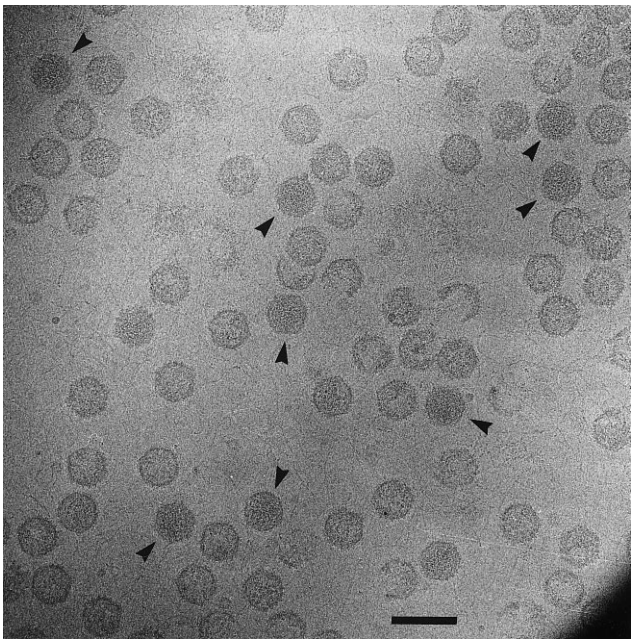

FIG. 1. Micrograph of IBDV particles in an unstained, frozen, hydrated preparation. Some of the particles (arrowheads) appear uniformly dark, but most appear blotchy, with the dark ring of the capsid standing out clearly. The former are likely to be complete particles with a full complement of RNA, whereas the latter have probably lost some or all of their RNA. Bar, 100 nm.

Individual three-dimensional maps were computed from particles coming from the same micrograph. The defocus value for each micrograph was determined by summing the intensities of the Fourier transforms of all of the particles selected from a particular micrograph, which was usually a greater number than was included in the final three-dimensional map, and by then using the positions of the minima observed. Maps from 10 different micrographs at different degrees of defocus were then combined, correcting for the contrast transfer function and allowing for 6% amplitude contrast (4). The resolution of the final maps was assessed by Fourier shell correlation or weighted phase residuals (20). The maps were displayed as surface-shaded representations by using the SURF program (21).

Because the capsid of IBDV proved to be markedly nonspherical, the density distribution within the thickness of the protein shell was not adequately displayed by sampling on simple spherical shells. We accordingly developed a program for sectioning of the map on faceted icosahedral shells, dividing each icosahedral face into three triangular facets. Each facet, corresponding to an asymmetric unit of the icosahedron, has two vertices on neighboring fivefold axes and one vertex on the threefold axis. By specifying the direction cosines of vectors to the corners of each facet plus a radial scale factor along each direction, it was possible to tilt the facets. In a regular icosahedron, the distances from the center at which the five-, two-, and threefold axis, respectively, intersect the surface are at a ratio of 1.176:1.0:0.934. In our faceted representation, based on a unit perpendicular distance of each facet from the center of the icosahedron, the corresponding distances at which the five-, two-, and threefold axes cut the faceted surface are 1.194, 1.015, and 1.004, respectively. In a depiction of the faceted sections (see Fig. 4), the radial distances specify the perpendicular distance of the facets from the center, and other distances can be calculated by multiplying by the appropriate factor.

## RESULTS

The appearance of IBDV particles when imaged in a frozen-hydrated but unstained state is shown in Fig. 1. The particle profiles are about 70 nm in diameter at their widest points. Some views have a noticeably angular shape, indicating that the capsid has marked departures from a spherical distribution. The contrast in the images of some particles is uniformly dark, but many others have a blotchy appearance, with the capsid appearing as a dark ring. The latter particles are likely to have lost some or all of their RNA, which can be seen as a fibrous network in the background. Other reports have noted the instability of some strains of IBDV on banding in CsCl (1, 14), and that seems to apply here too. We have made separate maps from images where the particles appear to be full and where they appear to be partly empty and could not detect any significant differences in the structure of the capsid between the two states. The map shown here was computed from a set of particles, the majority of which were partly empty, as there were then sufficient particles from each micrograph to allow production of individual maps and correction of the contrast

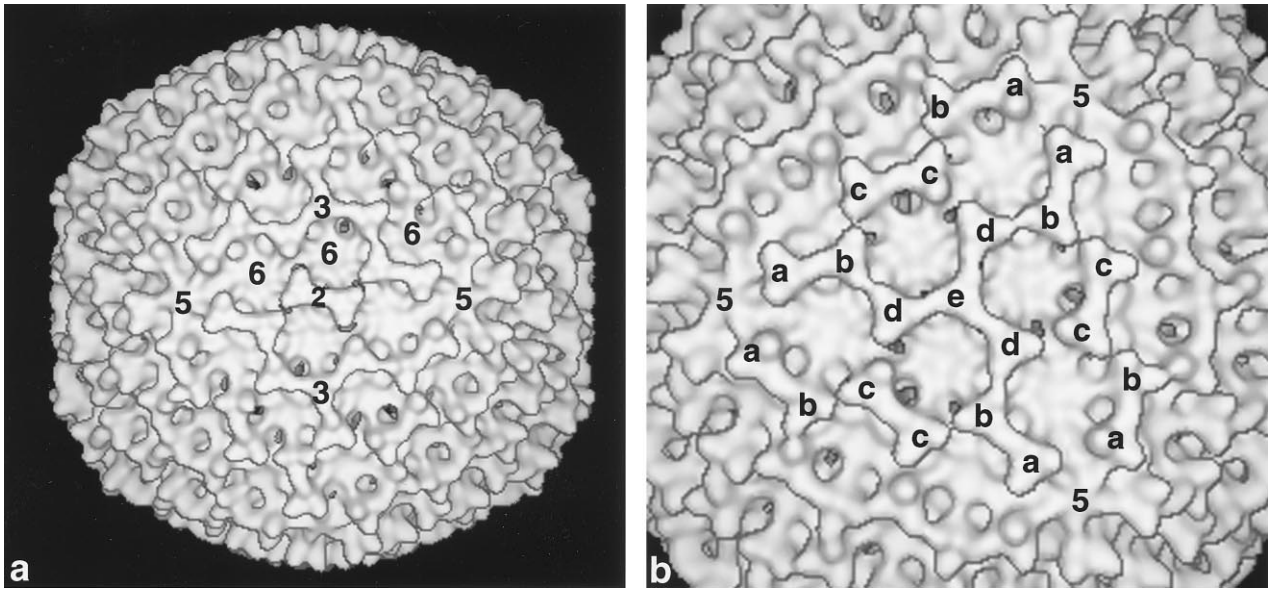


FIG. 2. Three-dimensional map of IBDV. (a) Twofold view of the whole particle. Some of the two-, three-, and fivefold and local sixfold axes are marked, and the pattern clearly indicates a T = 13 architecture. (b) Close-up view down the threefold axis of the particle, showing the trimer clustered nature of the packing at outer radii. The five symmetrically different classes of trimer are indicated by the letters a to e.

TABLE 1. Summary of micrographs

| Micrograph no. | Defocus (nm) | No. of particles |
|---|---|---|
| 2138 | 2,286 | 35 |
| 2144 | 2,035 | 29 |
| 2150 | 2,142 | 31 |
| 2189 | 1,570 | 35 |
| 2192 | 1,006 | 27 |
| 2194 | 1,559 | 29 |
| 2250 | 1,301 | 31 |
| 2260 | 507 | 17 |
| 2267 | 1,034 | 41 |
| 2268 | 1,226 | 65 |

transfer function (see Materials and Methods), resulting in higher resolution in the final map.

The three-dimensional map of IBDV (Fig. 2) shows that the capsid structure is organized with T=13 symmetry. At outermost radii, the trimer clustered subunits form triangular features that point towards each other. This creates a honeycomb pattern on the surface, and the disposition of the fivefold and local sixfold axes establishes the underlying T=13 symmetry (Fig. 2a). The T=13 lattice is skew, existing in left- and right-handed forms. From the experiments described here, it is not possible to determine the absolute hand of the lattice, so we have adopted the right-handed configuration (T=13d) indicated by surface shadowing (16). By splitting the set of particles into two subsets, computing two independent three-dimensional maps, and calculating the Fourier shell correlation, the resolution of the maps was shown to be about 1.8 nm (assessed as the Fourier spacing at which the weighted phase residual between the Fourier transforms of the maps rose to 70°). The final map shown here was computed from 340 particles taken from 10 different micrographs and has been icosahedrally averaged. The defocus value and number of contributing particles from each micrograph are shown in Table 1.

The 780 subunits in the outer part of the capsid form 260 trimer units, which lie in five different local environments labeled a to e (Fig. 2b). One class of trimer (class e) lies on the strict threefold axes of the whole particle and makes close contacts to the three neighboring trimers (class d). Other trimers make pairwise close contacts (e.g., a-b and c-c) that produce features like bowties, whereas there are gaps between c and d trimers and particularly between a and a trimers around the fivefold axes. The asymmetric unit of the structure consists of one-third of one of the strict trimers (class e) plus four other nonequivalent trimers (classes a to d), making a total of 13 subunits.

The intertrimer distances are correlated with the spherical radius at which the units lie. As already noted, the shell is nonisometric, with the units (class a) surrounding the fivefold axes extending to a 36-nm radius, the units (class e) at the threefold axes extending to a 33-nm radius, and the units (class c) next to the twofold axes extending to 33.5 nm. The surface trimers extend outwards by about 4 nm from a thin, nearly continuous shell, which closes off the holes at the five- and local sixfold axes (Fig. 2). The continuous shell is gently curved in most regions but is sharply bent at the fivefold axes (Fig. 3a). The line of the shell joining neighboring fivefold axes through the twofold position is almost straight (Fig. 3a), so that the continuous shell has the shape of an icosahedron but with slightly curved faces.

On the inner surface of the capsid, the trimer units appear as Y-shaped features, standing out from the continuous shell (Fig. 3a). There are only 200 of these Y-shaped features, as the 60 positions closest to the fivefold axes appear to be occupied by material which makes a rim around a pentagonal cavity at the fivefold position (Fig. 3b). The overall radial extent of the trimer unit is about 9 nm.

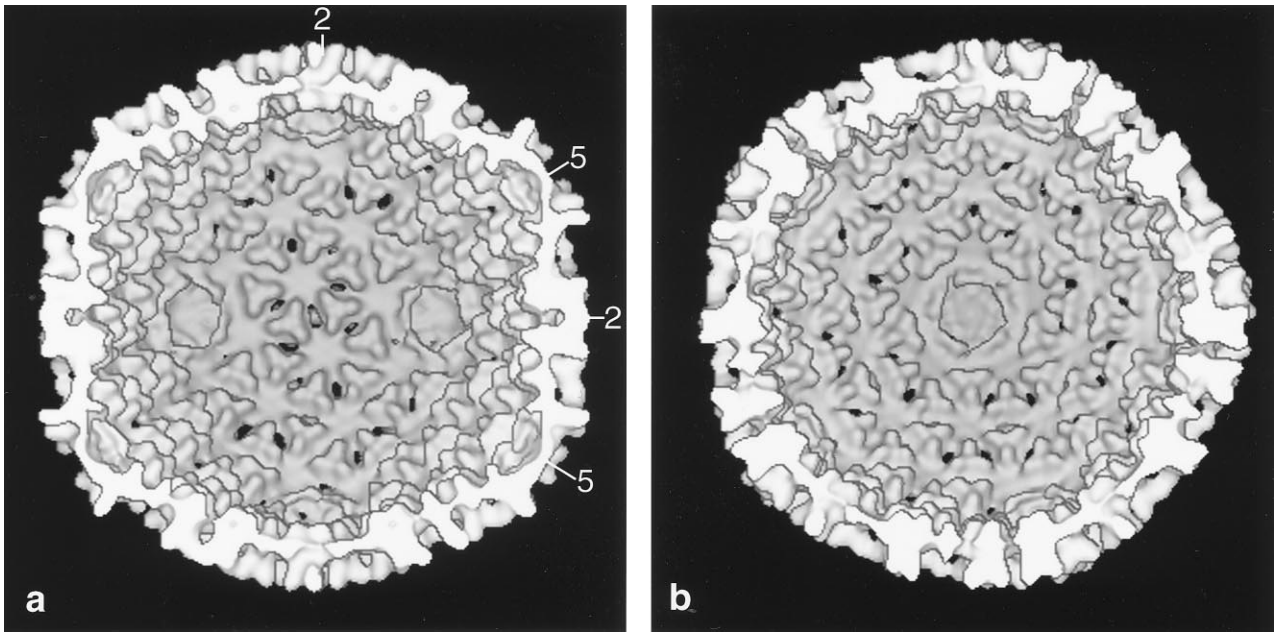


FIG. 3. Cutaway views showing the inner surface of the capsid of IBDV, viewed down the twofold axis (a) and the fivefold axis (b). A set of Y-shaped features indicates the trimer clustered packing of subunits, except at the positions closest to the fivefold axis. The equatorial slice in panel a (nearest to the viewer) contains two- and fivefold axes as indicated. The line section of the continuous shell running between fivefold axes through a twofold axis is almost straight, and the curvature is concentrated at the fivefold positions. In panel b, the rim surrounding the pentagonal cavity on the fivefold axis is clearly visible.

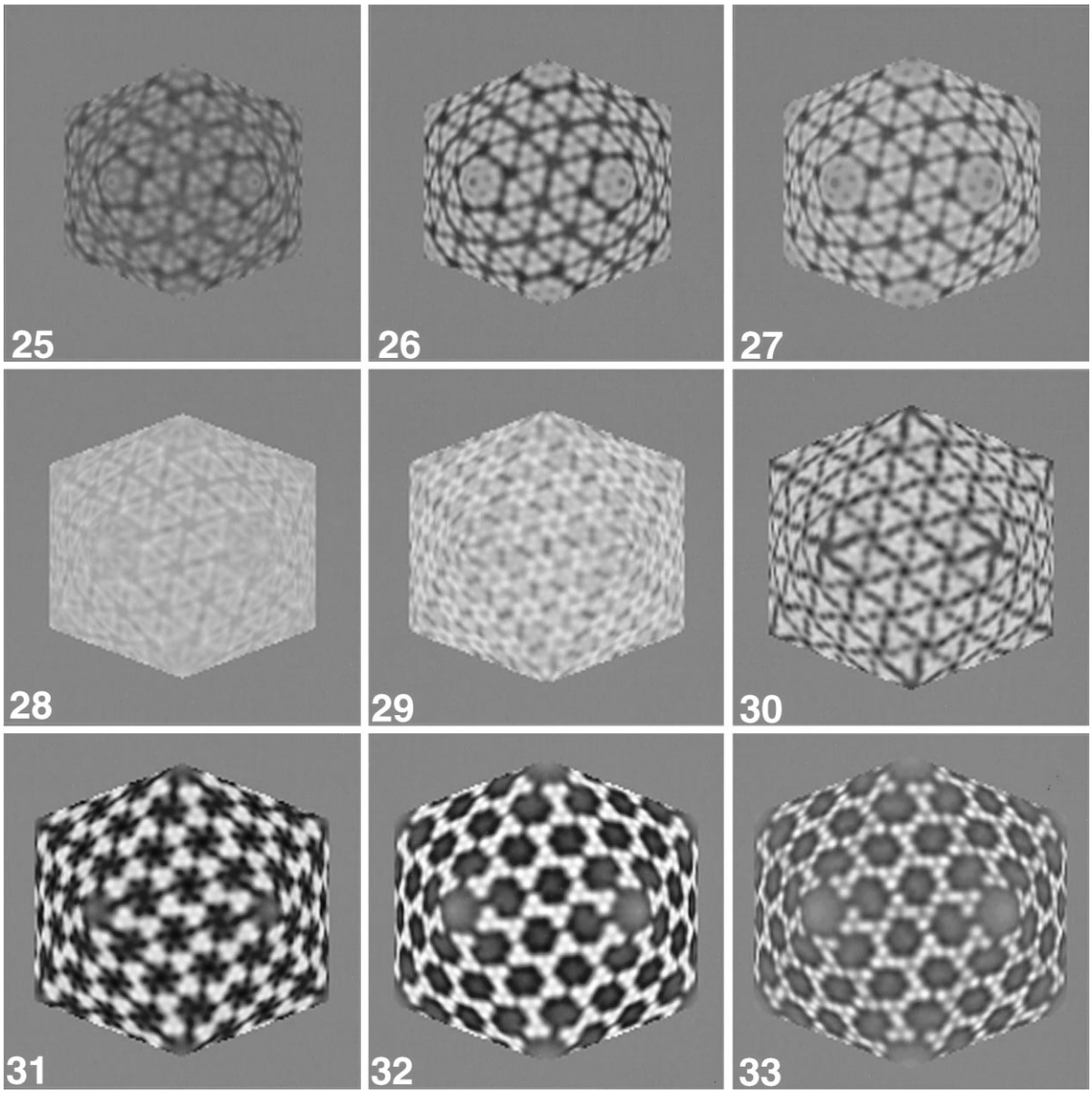


FIG. 4. Icosahedral sections of the three-dimensional map of IBDV viewed down a twofold axis. Because of the nonspherical shape of the capsid, it was essential to construct faceted icosahedral surfaces on which to display the density, so that equivalent parts of the subunits were equivalently sampled. The range of the sections shown is from 25 to 33 nm, with a radial step between sections of 1 nm, where the numbers refer to the perpendicular distances of the facets from the center of the particle (see Materials and Methods).

Because the capsid is nonisometric, it is essential to sample the density map on icosahedral sections (see the section on image processing in Materials and Methods) to see the equivalent features in the different subunits (Fig. 4). Simple spherical sections give a misleading impression of the subunit shape and density, especially for the subunits around the fivefold positions. The outermost sections (31 to 33 nm) show clearly the trimeric clustering of the subunits, with the tips of the subunits splayed slightly apart. Further in (30 nm), the trimers develop a triangular profile, with the vertices pointing towards the fivefold and local sixfold axes. At a 29-nm radius, there is additional material at the corners of the triangles which gives rise to pentameric and hexameric rings around the fivefold and local sixfold axes, respectively. This section, with the one at a 28-nm radius, forms the continuous shell. On the sections corresponding to the inner surface of the capsid (26 to 27 nm), the 200 Y-shaped features are clearly visible. However, the material immediately surrounding the fivefold axes has a different appearance, indicating either that the 60 Y-shaped features occupying these positions are very distorted or that these sites are occupied by a different protein. Thus, on sections from 29 to 33 nm, the material around all of the fivefold and local sixfold axes appears to be quasiequivalently packed, whereas on sections from 25 to 28 nm, the material around the fivefold axes appears not to be equivalent to that in the remainder of the shell.

To give an overall idea of the shape of the trimeric unit, we have cut out the strict trimer (class e) and three neighboring trimers (class d) (Fig. 5). The orientation of the trimers is such that on the outside of the capsid the triangles point roughly

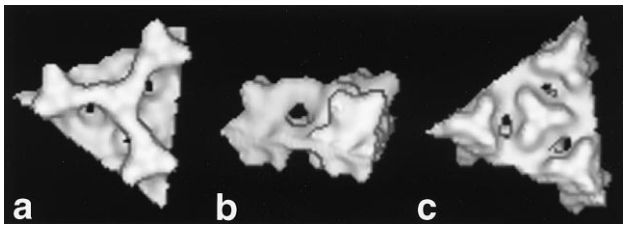


FIG. 5. Close-up view of the trimeric packing unit. A segment of the three-dimensional map has been cut out containing the trimer at a strict threefold axis (class e) and the three neighboring trimers (class d). This fragment of the structure is shown from outside the capsid (a), edge on (b), and from inside the capsid (c).

towards the twofold and local twofold axes, whereas on the inside of the capsid they point towards the local sixfold axes. From these detailed views, it can be seen that the outermost contact between class d and class e forms an arch. Under these arches, there appear to be small holes in the continuous shell at the positions of the local twofold axes relating the class d and class e trimers. Similar small holes are also found at the strict twofold axes relating class c trimers and at the local twofold axes relating class c to class b and at those relating class c to class d trimers.

## DISCUSSION

By analysis of frozen, hydrated, unstained specimens of IBDV, we have produced a three-dimensional map of the viral capsid at about 2 nm resolution. The map clearly establishes that the virus has T=13 symmetry, confirming an earlier report based on shadowed preparations (16), and shows that the subunits are predominantly trimer clustered. The capsid has marked departures from a spherical distribution, with the units near the fivefold axes extending to a radius of about 36 nm, whereas those at the threefold axes extend only to 33 nm. The outer parts of the trimer units have different environments, with some neighbors making close contacts while others are far apart. The outer parts of the 260 trimers protrude from an almost continuous shell of density (radius, 28 to 30 nm) in which the packing of the subunits appears to be more equivalent. On the inner surface of the capsid, the trimers form Y-shaped features but there are only 200 of these, as the 60 that would surround the fivefold axes appear to be missing. Instead, there is a rim of material which marks out a pentagonal cavity on each fivefold axis.

Analysis of the protein composition of IBDV has shown that VP2 constitutes 51%, VP3 constitutes 40%, VP4 constitutes 6%, and VP1 constitutes 3% of the protein in the infectious virus (9, 14). VP2 and VP3 are thus major structural components of the virus. VP2 carries neutralizing epitopes and is thus likely to be exposed on the surface of the virus (1, 2). VP3 has a basic C-terminal region of the kind expected to interact with the RNA (13) and is therefore likely to be either on the inner surface of the capsid or internally packaged with the RNA. A possible interpretation of the features seen in the three-dimensional map is therefore that the outer part of the capsid (radii of 29 to 33 nm) is formed from VP2. The Y-shaped features seen on the inside of the capsid (radii of 26 to 28 nm) could be formed by part of VP3, with the basic region extending inwards to interact with the RNA. This part of the protein is likely to be disordered and therefore not visualized in the icosahedrally averaged map. The material forming the rim around each fivefold axis on the inner surface of the capsid might then correspond to VP4. This model of the virion would predict that there would be 780 copies of VP2, 600 copies of VP3, and 60 copies of VP4, numbers roughly in line with the observed composition. The total molecular mass expected in the capsid shell for this model would be approximately 50 MDa ($780 \times 40$ kDa + $600 \times 28$ kDa + $60 \times 28$ kDa), allowing for the fact that the tails of the VP3 molecules are likely to be disordered. This corresponds to a volume $6 \times 10^7$ Å$^3$. The surfaces in the maps shown have been generated to include approximately 80% of this volume to give clear definition to the features. Surface representations at a level corresponding to 100% look almost identical, although some of the small holes seen in the maps tend to fill. The findings presented here are not sensitive to the exact level selected.

The general form of T=13 trimer clustered architecture found in IBDV is also seen in the inner shells of viruses in the *Reoviridae* family, although the virus structures themselves are much more complex than that of IBDV. In rotavirus (17) and bluetongue virus (18), the so-called single-shelled particles show projecting spikes at the threefold and local threefold positions, although the spike profiles are not as strongly triangular as those we observed in IBDV. Moreover, in rotavirus and bluetongue virus there are large, open channels at the fivefold and local sixfold positions, whereas in IBDV these positions are closed off by the material in the continuous shell. The structure of the bluetongue virus VP7 trimer is known in atomic detail (12). Reovirus is also based on T=13 architecture (15), but a complex set of structural rearrangements accompany the maturation of the virion (10). In the intermediate subviral particle, the shape and disposition of the trimers are quite like those in IBDV but there are special structures on the fivefold axes (10). It has not proved possible to detect any sequence homology between the trimer-forming proteins of IBDV, rotavirus, bluetongue virus, and reovirus, so it appears that this general architecture can be realized by proteins with quite different sequences.

## ACKNOWLEDGMENTS

This work was supported in part by grant 96-04-48894 from the Russian Foundation for Basic Science Investigations (N.A.K. and V.Y.S) and by an EEC Human Capital and Mobility grant (ERB4001 GT931348) (B.B.). A travel grant from the Royal Society of London is gratefully acknowledged (N.A.K.).

We thank M. A. Skinner for helpful comments on the manuscript.

## REFERENCES

1. **Azad, A. A., M. N. Jagadish, M. A. Brown, and P. J. Hudson.** 1987. Deletion mapping and expression in *Escherichia coli* of the large genomic segment of a birnavirus. Virology **161:**145–152.
2. **Becht, H., H. Müller, and H. K. Müller.** 1988. Comparative studies on structural and antigenic properties of two serotypes of infectious bursal disease virus. J. Gen. Virol. **69:**631–640.
3. **Bellare, J. R., H. T. Davis, L. E. Scriven, and Y. Talmon.** 1988. Controlled environment vitrification system: an improved sample preparation technique. J. Electron Microsc. Tech. **10:**87–111.
4. **Böttcher, B., and R. A. Crowther.** 1996. Difference imaging reveals ordered regions of RNA in turnip yellow mosaic virus. Structure **4:**387–394.
5. **Brown, F.** 1986. The classification and nomenclature of viruses: summary of results of meetings of the International Committee on Taxonomy of Viruses in Sendai, September 1984. Intervirology **25:**141–143.
6. **Chettle, N., J. C. Stuart, and P. J. Wyeth.** 1989. Outbreak of virulent infectious bursal disease in East Anglia. Vet. Rec. **125:**271–272.
7. **Crowther, R. A.** 1971. Procedures for three-dimensional reconstruction of spherical viruses by Fourier synthesis from electron micrographs. Philos. Trans. R. Soc. Lond. Biol. Sci. **261:**221–230.
8. **Crowther, R. A., N. A. Kiselev, B. Böttcher, J. A. Berriman, G. P. Borisova, V. Ose, and P. Pumpens.** 1994. Three-dimensional structure of hepatitis B virus core particles determined by electron cryomicroscopy. Cell **77:**943–950.
9. **Dobos, P., B. J. Hill, R. Hallett, D. T. C. Kells, H. Becht, and D. Teninges.** 1979. Biophysical and biochemical characterization of five animal viruses with bisegmented double-stranded RNA genomes. J. Virol. **32:**593–605.

10. **Dryden, K. A., G. Wang, M. Yeager, M. L. Nibert, K. M. Coombs, D. B. Furlong, B. N. Fields, and T. S. Baker.** 1993. Early steps in reovirus infection are associated with dramatic changes in supramolecular structure and protein conformation: analysis of virions and subviral particles by cryoelectron microscopy and image reconstruction. J. Cell Biol. **122:**1023–1041.
11. **Dubochet, J., M. Adrian, J.-J. Chang, J.-C. Homo, J. Lepault, A. W. McDowall, and P. Shultz.** 1988. Cryo-electron microscopy of vitrified specimens. Q. Rev. Biophys. **21:**129–228.
12. **Grimes, J., A. K. Basak, P. Roy, and D. Stuart.** 1995. The crystal structure of bluetongue virus VP7. Nature **373:**167–170.
13. **Hudson, P. J., N. M. McKern, B. E. Power, and A. A. Azad.** 1986. Genomic structure of the large RNA segment of infectious bursal disease virus. Nucleic Acids Res. **14:**5001–5012.
14. **Kibenge, F. S. B., A. S. Dhillon, and R. G. Russell.** 1988. Biochemistry and immunology of infectious bursal disease virus. J. Gen. Virol. **69:**1757–1775.
15. **Metcalf, P., M. Cyrklaff, and M. Adrian.** 1991. The three-dimensional structure of reovirus obtained by cryo-electron microscopy. EMBO J. **10:** 3129–3136.
16. **Özel, M., and H. Gelderblom.** 1985. Capsid symmetry of viruses of the proposed birnavirus group. Arch. Virol. **84:**149–161.
17. **Prasad, B. V. V., G. J. Wang, J. P. M. Clerx, and W. Chiu.** 1988. Three-dimensional structure of rotavirus. J. Mol. Biol. **199:**269–275.
18. **Prasad, B. V. V., S. Yamaguchi, and P. Roy.** 1992. Three-dimensional structure of single-shelled bluetongue virus. J. Virol. **66:**2135–2142.
19. **Van den Berg, T. P., M. Gonze, and G. Meulemans.** 1991. Acute infectious bursal disease in poultry: isolation and characterisation of a highly virulent strain. Avian Pathol. **20:**133–143.
20. **van Heel, M.** 1987. Similarity measures between images. Ultramicroscopy **21:**95–100.
21. **Vigers, G. P. A.** 1986. Clathrin assemblies in vitreous ice. Ph.D. thesis. University of Cambridge, Cambridge, England.